J. Membrane Biol. 156, 173–190 (1997)

The Journal of
Membrane
Biology

Gating and Conduction Properties of a Sodium-activated Cation Channel from Lobster Olfactory Receptor Neurons

A.B. Zhainazarov,[1] B.W. Ache[1,2]

[1]Whitney Laboratory, University of Florida, 9505 Ocean Shore Blvd., St. Augustine, FL 32086, USA
[2]Departments of Zoology and Neuroscience, University of Florida, Gainesville, FL 32610, USA

Received: 17 September 1996/Revised: 15 November 1996

Abstract. The gating and conduction properties of a channel activated by intracellular Na^+ were studied by recording unitary currents in inside-out patches excised from lobster olfactory receptor neurons. Channel openings to a single conductance level of 104 pS occurred in bursts. The open probability of the channel increased with increasing concentrations of Na^+. At 210 mM Na^+, membrane depolarization increased the open probability e-fold per 36.6 mV. The distribution of channel open times could be fit by a single exponential with a time constant of 4.09 msec at −60 mV and 90 mM Na^+. The open time constant was not affected by the concentration of Na^+, but was increased by membrane depolarization. At 180 mM Na^+ and −60 mV, the distribution of channel closed times could be fit by the sum of four exponentials with time constants of 0.20, 1.46, 8.92 and 69.9 msec, respectively. The three longer time constants decreased, while the shortest time constant did not vary with the concentration of Na^+. Membrane depolarization decreased all four closed time constants. Burst duration was unaffected by the concentration of Na^+, but was increased by membrane depolarization. Permeability for monovalent cations relative to that of Na^+ (P_X/P_{Na}), calculated from the reversal potential, was: Li^+ (1.11) > Na^+ (1.0) > K^+ (0.54) > Rb^+ (0.36) > Cs^+ (0.20). Extracellular divalent cations (10 mM) blocked the inward Na^+ current at −60 mV according to the following sequence: Mn^{2+} > Ca^{2+} > Sr^{2+} > Mg^{2+} > Ba^{2+}. Relative permeabilities for divalent cations (P_Y/P_{Na}) were Ca^{2+} (39.0) > Mg^{2+} (34.1) > Mn^{2+} (15.5) > Ba^{2+} (13.8) > Na^+ (1.0). Both the reversal potential and the conductance determined in divalent cation-free mixtures of Na^+ and Cs^+ or Li^+ were monotonic functions of the mole fraction, suggesting that the channel is a single-ion pore that behaves as a multi-ion pore when the current is carried exclusively by divalent cations. The properties of the channel are consistent with the channel playing a role in odor activation of these primary receptor neurons.

Key words: Lobster — Patch clamp — Electrophysiology — Single-channel recording — Sodium-activated cation channel

Introduction

A growing family of potassium-selective ion channels are those activated by intracellular Na^+. They occur in cardiac myocytes (Kameyama et al., 1984), crayfish motorneurons (Hartung, 1985), chick ciliary and trigeminal neurons (Bader, Bernheim & Bertrand, 1985; Haimann et al., 1990), chick midbrain neurons (Dryer, Fujii & Martin, 1989), cat neocortical neurons (Schwindt, Spain & Crill, 1989), rat olfactory bulb neurons (Egan et al., 1992*a*), *Xenopus* oocytes (Egan et al., 1992*b*), *Xenopus* spinal neurons (Dale, 1993), and insect neurosecretory cells (Grolleau & Lapied, 1994). The presence of these channels in a variety of cell types from diverse tissues indicates that Na^+-activated potassium channels potentially play an important role in cell function. It has been proposed that these channels might participate in the regulation of cell excitability, but their physiological function(s) remains to be determined (review: Dryer, 1994).

Intracellular Na^+ also activates ion channels that are nonselective for cations. Na^+-sensitive nonselective cation channels occur in peptidergic nerve terminals in crabs (Stuenkel et al., 1990), on the soma of cultured lobster olfactory receptor neurons (Zhainazarov & Ache, 1995*a*), and on mammalian intestinal myocytes (Nouail-

Correspondence to: A.B. Zhainazarov

hetas et al., 1994). A Na^+-activated transient nonselective cationic current in frog tectal neurons (Zaykin & Nistri, 1995), may reflect the presence of a similar unitary current in amphibians, as well. Like their K^+-selective counterparts, these nonselective cation channels presumably form another family of Na^+-activated, or at least Na^+-sensitive, channels whose functional role is also unknown. The lobster Na^+-activated nonselective cation channel occurs at the site of odor transduction in the outer dendrites of primary olfactory receptor neurons (ORNs) *in situ* (Zhainazarov & Ache, 1996), suggesting that the channel's function is somehow associated with this highly specialized cellular compartment. Indeed, the channel contributes to the generation of a substantial part of the depolarizing receptor potential (A.B. Zhainazarov, R. Doolin & B.W. Ache, *in preparation*), suggesting that the channel may be secondarily activated by Na^+ influx through the primary odor transduction channel and serve to amplify the primary transduction current. To rigorously understand the function of this channel, however, we need to better understand the channel's gating behavior and conduction properties.

Here, we characterize the detailed kinetic properties of the Na^+-activated nonselective cation channel from cultured lobster ORNs and the effects of changes in membrane potential and $[Na^+]_i$ on channel gating. We also describe the conduction properties of the channel, including its selectivity for monovalent and divalent cations, blocking by extracellular divalent cations of the current carried by Na^+, dependence of the channel conductance on the permeant ion concentration, and the mole-fraction behavior of the single-channel current. We show that the Na^+-activated channel is relatively nonselective among monovalent cations and highly permeable to all of five divalent cations tested. Part of this work appeared previously in abstract form (Zhainazarov & Ache, 1996).

Materials and Methods

Preparation

Unitary currents were obtained from cell-free, inside-out membrane patches pulled from the somata of cultured spiny lobster (*Panulirus argus*) ORNs. Animals were collected in the Florida Keys and maintained in the laboratory in running seawater on a mixed diet of frozen fish, squid, and shrimp. ORNs were maintained in primary culture as described earlier (Fadool, Michel & Ache, 1991) and used within 1–7 days of culture. Coverslips containing the cells were transferred to a *Panulirus* saline-filled 35 mm diameter culture dish (Falcon 1008, Becton Dickinson) mounted on the stage of an inverted microscope (Axiovert 100, Carl Zeiss) and viewed with phase-contrast optics at 320× magnification. ORNs were identified in the culture by their morphology and electrophysiological properties, as described earlier (Fadool, Michel & Ache, 1993).

Recording

Patch-clamp recordings were made as described by Hamill et al. (1981). Patch pipettes were fabricated from borosilicate glass (Sutter Instrument BF150-86-10), coated with silicone elastomer (Sylgard; Dow-Corning) and fire-polished to a final tip diameter <1 μm. The pipettes had resistances of 10–20 MΩ when filled with patch pipette solution and formed seals with resistances of 20–25 GΩ. After forming a gigaseal and excising the membrane patch into *Panulirus* saline, the pipette was moved immediately in front of one tube of a nine-channel rotatory parallel flow perfusion system (RSC-100, Biologic) placed in the culture dish. Stimulus solution continuously flowed from the tube (100 μm, inner diameter) and completely engulfed the patch. The remaining identical eight tubes either contained stimulus solution or a modified or drug-containing solution appropriate to the particular experiment. Electronically switching another of the tubes in front of the stationary pipette ''concentration clamped'' the patch in a new solution in 10 msec. Unitary currents were recorded with a commercial amplifier (Axopatch 200A, Axon Instruments), low-pass filtered at 10 kHz (−3 dB; 4-pole Bessel filter), and stored on videotape (Toshiba DX-900) for later analysis. All potentials were corrected for the liquid junction potentials between the pipette and bath solutions as described by Neher (1992). The recordings were referenced to a Ag-AgCl wire electrode connected to the bath solution through a 3 M KCl/agar bridge. All experiments were carried out at room temperature (20–22°C).

Data Analysis

On playback from videotape, the single channel current records were filtered at 2–4 kHz (−3 dB; 8-pole Bessel filter) and digitized at 20–40 kHz by a IBM-compatible computer with an A/D, D/A interface (TL-1, Axon Instruments) using commercially-available software (pClamp 6.0, Axon Instruments). An idealized record of the durations and amplitudes of detectable events in the single channel current record was obtained by imposing a fixed resolution (50 μsec) for both open and closed times (Colquhoun & Sigworth, 1995). Only openings with a duration equal to or longer than 2 t_r were included in amplitude histograms, where t_r is the rise time of recording system. Amplitude histograms were binned into equally spaced bins and fitted with the sum of several Gaussian components using the method of least squares minimization. Histograms of the distribution of open times and closed times, and parameters of bursts of openings were displayed as the logarithm of the duration with a square root transformation of the ordinate. Dwell-time distributions were fitted with the sum of several exponential components by using the method of maximum likelihood and the best fit was determined statistically (F-statistic, $\alpha < 0.01$) comparing the results of fitting with different number of components.

Channel openings typically occurred in groups. We classified the groups of openings as bursts of openings using the following criteria. Bursts of openings were defined as a group of openings separated by closed times shorter than a critical time interval t_c (Colquhoun & Sigworth, 1995). The value of t_c for bursts was determined so that the number of long closed times (second component in all closed times distribution) that were misclassified as occurring within bursts equals the number of short closed times (first component in all closed times distribution) that were misclassified as occurring between bursts (Colquhoun & Sakmann, 1985; Colquhoun & Sigworth, 1995).

In some experiments the current-voltage relation of single-channel currents was determined by the application of voltage ramps (−70 to +50 mV; 300 msec), and the resulting currents recorded directly into computer memory and analyzed later by using the segmented averaging procedure (Heinemann, 1995). The reversal potentials under different ionic conditions for monovalent cations were mea-

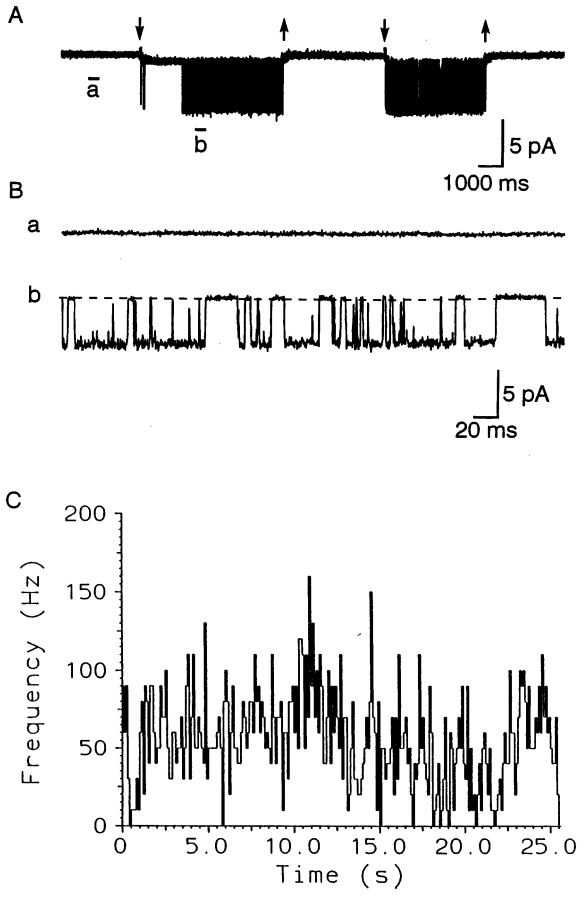

Fig. 1. Na^+ directly activates a channel in an inside-out patch from the soma of a cultured lobster olfactory receptor neuron. (*A*) Inside-out patch bathed in 0 mM NaCl/210 mM LiCl solution had no channel activity, but showed reversible channel activity when transferred into 210 mM NaCl/0 mM LiCl solution. The patch contained only one Na^+-activated channel. Time course of solution change is shown by solid arrows above the current trace. (*B*) Segments taken from the trace in A (*a* and *b*) and shown on an expanded time scale. Channel openings appear as downward deflections. (*C*) frequency of Na^+-activated channel openings as a function of time. $[Na^+]_i$, 210 mM. Frequency was calculated over a time interval lasting 100 msec *A* and *C* are from different patches. Membrane potential, −60 mV. Low-pass filtered at 2 kHz (−3 dB).

sured by determining the potential at which the open channel current was zero. The permeability of test monovalent ion X^+ relative to Na^+ (P_X/P_{Na}) was calculated from the shift of the reversal potential (E_r) upon exchanging the intracellular Na^+ solution (210 mM)—which contained no other monovalent, permeant cations—with an identical solution, except that part of the Na^+ (120 mM) was replaced by an equivalent concentration of test cation X^+ by using the Goldman-Hodgkin-Katz potential equation (Hille, 1992):

$$\Delta E_r = E_{r,X} - E_{r,Na} = (RT/F)ln\{P_{Na}[Na^+]_o/(P_X[X^+]_i + P_{Na}[Na^+]_i)\}, \quad (1)$$

where R is the gas constant, F the Faraday constant, T the absolute temperature, $[Na^+]_o$ the extracellular concentration of Na^+, $[X^+]_i$ and $[Na^+]_i$ the intracellular concentration of the cations X^+ and Na^+ respectively.

In some experiments, estimation of the permeability of the divalent cation Y^{2+} (105 mM, pipette solution) relative to Na^+ (210 mM, bath solution) (P_Y/P_{Na}) was based on the value of E_r and calculated by using the equation (Fatt & Ginsborg, 1958):

$$P_Y[Y^{2+}]_o/P_{Na}[Na^+]_i = \exp(E_rF/RT)[\exp(E_rF/RT) + 1]/4, \quad (2)$$

where $[Y^{2+}]_o$ is the extracellular concentration of the divalent cation Y^{2+}.

Solutions

Unless noted otherwise, standard patch pipette solution consisted of (in mM): 210 NaCl, 11 EGTA, 1 $CaCl_2$, 10 HEPES, and 696 glucose, at a pH of 7.4 adjusted with tris(hydroxymethyl) aminomethane (Tris base). The estimated free calcium concentration in the pipette solution was 10 nM. Free calcium concentration was calculated with the use of Chelator software (Schoenmaker et al., 1992). *Panulirus* saline consisted of (in mM): 458 NaCl, 13.4 KCl, 13.4 Na_2SO_4, 13.6 $CaCl_2$, 9.8 $MgCl_2$, 2 glucose, 10 HEPES, at a pH of 7.4 adjusted with Tris base. Stimulus solution consisted of (in mM): 210 LiCl, 11 EGTA, 1 $CaCl_2$, 696 glucose, and 10 HEPES, at a pH of 7.4 adjusted with Tris base. In some experiments, part of the LiCl in the stimulus solution was substituted by an equivalent concentration of NaCl, as described in the text and figure legends. In experiments carried out to determine the extent of blockage of the channel by different divalent cations, the patch pipette solution consisted of (in mM) 190 NaCl, 10 Na-acetate, 10 HEPES, 696 glucose, and one of the following divalent cation chlorides: $CaCl_2$, $MgCl_2$, $BaCl_2$, $SrCl_2$, and $MnCl_2$, pH 7.4 adjusted with Tris base. In experiments performed to measure divalent permeation through the channel, the patch pipette solution consisted of (in mM) 10 HEPES, and 105 chloride of one of the following divalent cations: Ca^{2+}, Mg^{2+}, Ba^{2+}, Sr^{2+}, and Mn^{2+}, pH 7.4 adjusted with Tris base and at ~1000 mmol/kg osmolarity adjusted with glucose.

All inorganic salts were obtained from Fisher Scientific. All organic chemicals were obtained from Sigma Chemical except for HEPES, which was obtained from Research Organics.

Results

As shown previously (Zhainazarov & Ache, 1995*a*), Na^+ directly and reversibly activated unitary currents when applied to the intracellular side of the membrane (Fig. 1*A* and *B*), and did so without desensitization (Fig. 1*C*). Of 81 patches tested in this study, 65 showed Na^+-activated channel activity. The majority of these contained multiple channels (range 1–9, mean 6), as determined by counting multiple openings at a high $[Na^+]_i$ (210 mM). Ten of the patches contained only one channel by this criterion and were used for dwell-time analysis.

Amplitude of Na^+-activated Channel Openings

In the presence of Na^+, the channel opened to a single level of −5.82 ± 0.35 (SD) pA at −60 mV (Fig. 2*A*) in all but one of the 65 patches with Na^+-activated channel activity. In one patch a second substate opening with an

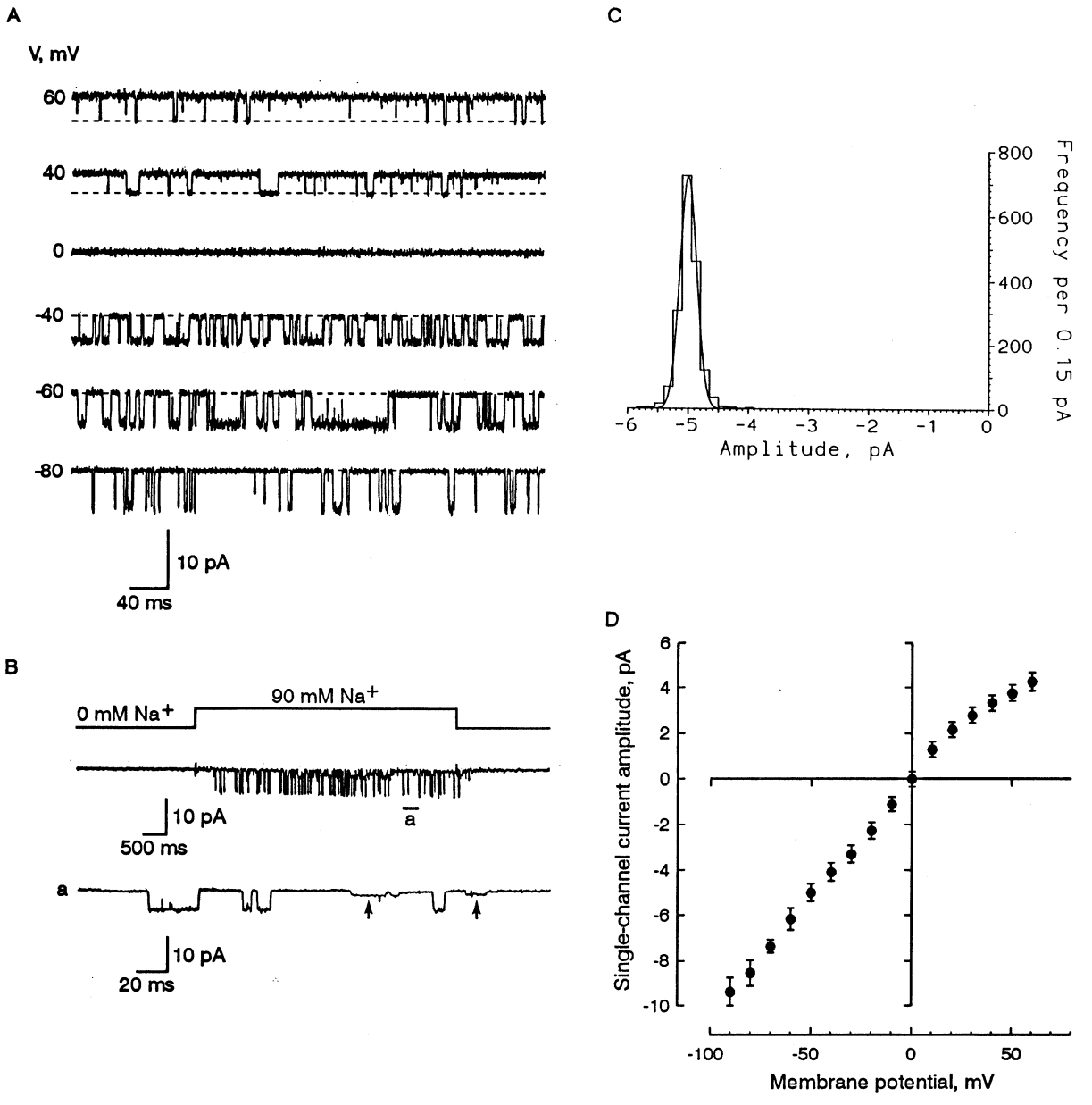

Fig. 2. Single-channel current traces from inside-out patch containing only one Na^+-activated channel at different membrane potentials. Value of membrane potential is shown near each trace. Baselines are depicted by dashed lines. $[Na^+]_i$, 210 mM. $[Na^+]_o$, 210 mM. The current traces were low-pass filtered at 2 kHz (−3 dB). (*B*) In one patch 90 mM Na^+-activated reversibly a channel with a substate opening in addition to the main open one. The solid line above the current trace indicates time course of solution change. Arrows indicate putative substate openings. Membrane, −60 mV. Low-pass filtered at 2 kHz (−3 dB). (*C*) Amplitude histogram of 1754 openings longer than 0.332 ms obtained from the same patch as shown in *A*. The solid line is the fit of one Gaussian function with following parameters of (mean ± SD): −5.00 ± 0.14 pA. Membrane potential, −50 mV. (*D*) Current-voltage relationship of single Na^+-activated channel current amplitude. The mean single channel current amplitude at each membrane potential was obtained from single Gaussian fit to the amplitude histogram. Points are given as the mean ± SD ($n = 5$). $[Na^+]_i$, 210 mM. $[Na^+]_o$, 210 mM.

amplitude of −1.10 ± 12 (SD) pA at −60 mV (Fig. 2*B*) was seen, but was not analyzed further due to its rare occurrence. The amplitude distribution of channel opening at 210 mM Na^+ and −50 mV could be fit with a single Gaussian function with parameter of −5.00 ± 0.14 (mean ± SD) pA (Fig. 2*C*). The current-voltage relationship of open channel current amplitude was linear over negative membrane potentials and showed slight inward rectification at positive potentials (Fig. 2*D*). The slope conductance of the channel was 103.9 ± 5.2 (SD) pS ($n = 5$) between −90 and 10 mV, with a reversal potential of −0.4 ± 0.1 (SD) mV.

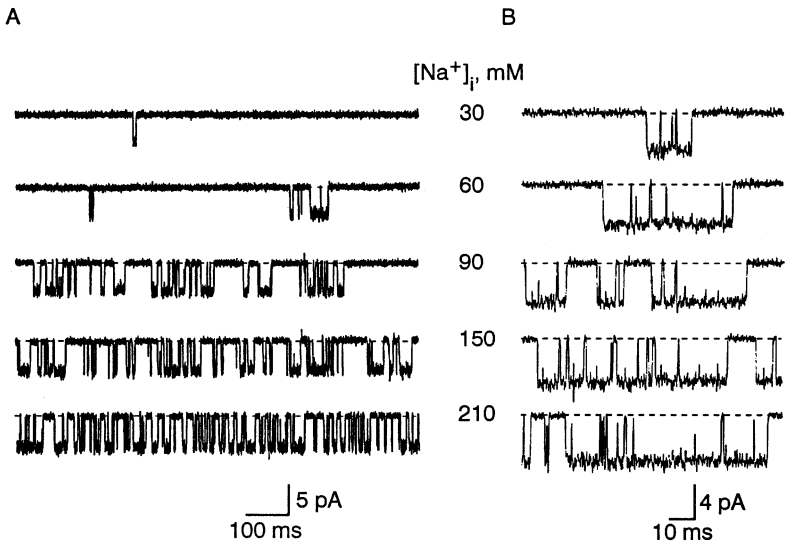

Fig. 3. (*A*) Samples of single Na^+-activated channel currents at various $[Na^+]_i$ (30 mM to 210 mM). (*B*) Segments taken from the traces in *A* shown on an expanded time scale. Baselines are depicted by dashed lines. Channel openings are shown as downward deflections. The patch contained only one Na^+-activated channel. Membrane potential was clamped at −60 mV. The currents were low-pass filtered at 2 kHz (−3 dB).

Concentration Dependence of the Open Probability

Channel activity increased in concentration-dependent manner as $[Na^+]_i$ was increased from 30 to 210 mM (Fig. 3). Channel openings were grouped into bursts even at low $[Na^+]_i$. The channel continued to show such bursting behavior at higher $[Na^+]_i$, although the bursts of openings were separated by much shorter periods of channel closings than at low $[Na^+]_i$ (Fig. 3). It is unlikely that such bursting behavior resulted from divalent ion block since in all our solutions free Ca^{2+} concentration was buffered at 10 nM by 11 mM EGTA, and the solutions contained no added Mg^{2+}.

The open probability of the channel (P_o) calculated as the proportion of total time spent in the open state increased from 0.02 ± 0.01 (SEM) to 0.54 ± 0.02 (SEM) (n = 6) at −60 mV as the $[Na^+]_i$ was elevated from 30 to 210 mM (○ points, Fig. 4*A*). The data could be fit by the Hill equation:

$$P_o = P_{o,\,max}\,[Na^+]_i^n/(K_{1/2}^n + [Na^+]_i^n), \qquad (3)$$

where $P_{o,\,max}$ (0.58 ± 0.03 (SEM)) is an asymptotic value of channel P_o, n is the Hill coefficient (3.10 ± 0.09 (SEM)), and $K_{1/2}$ is a half-effect concentration (89.2 ± 4.2 (SEM) mM).

When the patch was voltage-clamped at +40 mV, the open probability of the channel increased from 0.07 ± 0.02 (SEM) at 30 mM Na^+ to 0.96 ± 0.02 (SEM) (n = 6) at 210 mM (• points, Fig. 4*A*). The Hill equation fit to the data points gave the following parameters. $P_{o,\,max}$ increased from 0.58 at −60 mV to 0.96 ± 0.01 (SEM) at +40 mV, indicating that the fully ligand-bound channel has a higher open probability at positive potentials. At both negative and positive membrane potentials the Hill coefficient value was greater than 3 (3.25 ± 0.21 (SEM) at −60 mV and 3.10 ± 0.09 (SEM) at +40 mV). $K_{1/2}$ decreased from 89.2 ± 4.2 (SEM) at −60 mV to 45.3 ± 1.1 (SEM) at +40 mV, suggesting that the rate constants of the Na^+ binding stages of the channel are also voltage-dependent.

Voltage Dependence of the Open Probability

The channel P_o clearly increased when the membrane potential was gradually changed from negative to positive potentials, even if $[Na^+]_i$ was at saturating level (210 mM) (• points, Fig. 4*B*). For example, P_o was 0.21 ± 0.02 (SEM) at −90 mV and 0.94 ± 0.03 (SEM) (n = 6) at +60 mV, suggesting that the fully ligand-bound channel has a higher open probability at positive potentials. The solid line through the data (• points, Fig. 4*B*) was drawn according to the Boltzmann equation:

$$P_o = P_{o,\,max}/(1 + \exp((V_{1/2} - V)/k), \qquad (4)$$

where $P'_{o,\,max}$ is the asymptotic value of P_o, $V_{1/2}$ is the membrane potential at which half of $P'_{o,\,max}$ is reached, and k is the slope factor describing the steepness of the relationship. At saturating $[Na^+]_i$ (210 mM) the fit parameters were $P_{o,\,max}$ 1.00 ± 0.03 (SEM), $V_{1/2}$ −42.1 ± 3.4 (SEM) mV, and k 36.6 ± 3.2 (SEM) mV.

When the inside of the patch was bathed in a non-saturating $[Na^+]_i$ (90 mM), the channel activity was still voltage-dependent (○ points, Fig. 4*B*). The channel P_o increased from 0.05 ± 0.03 (SEM) at −90 mV to 0.86 ± 0.03 (SEM) (n = 6) at +60 mV. $P'_{o,\,max}$ (0.96 ± 0.07 (SEM)) and k (29.0 ± 4.7 (SEM) mV) did not change in comparison with their values at 210 mM $[Na^+]_i$. In contrast, $V_{1/2}$ changed considerably (−11.7 ± 7.3 (SEM) mV),

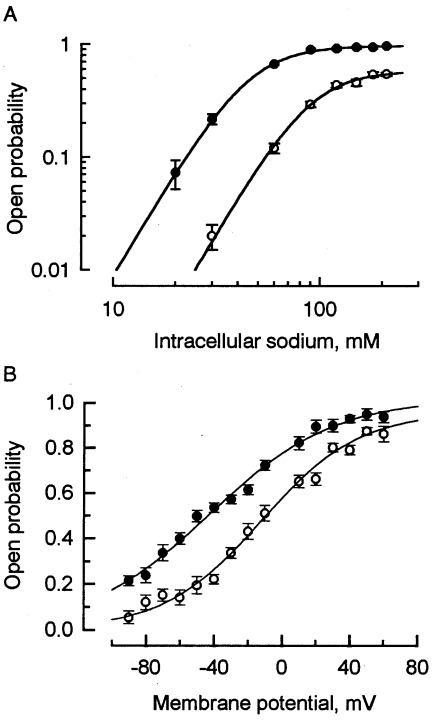

Fig. 4. (*A*) Relationship between $[Na^+]_i$ and open probability of single Na^+-activated channels at two different membrane potentials (○, −60 mV; ●, +40 mV). In *A* the solid lines were drawn according to the Hill equation with parameters of: the asymptotic value of open probability $P_{o,\,max}$ (0.96 ± 0.01, +40 mV; 0.58 ± 0.03, −60 mV), the Hill coefficient n (3.10 ± 0.09, +40 mV; 3.25 ± 0.21, −60 mV), and the half-effect concentration $K_{1/2}$ (45.3 ± 1.1, +40 mV; 89.2 ± 4.2, −60 mV). (*B*) Voltage dependence of P_o measured at two different value of $[Na^+]_i$ (○, 90 mM; ●, 210 mM). Membrane potential ranted from −90 mV to +60 mV. In *B* solid lines show the fit of the Boltzmann equation (*see text*) to the data. Fit of Boltzmann equation to data points yielded $P'_{o,\,max}$ = 1.02 ± 0.03, $V_{1/2}$ = −42.1 ± 3.4 mV, k = 36.6 ± 3.2 mV ($[Na^+]_i$ = 210 mM) and $P'_{o,\,max}$ = 0.96 ± 0.07, $V_{1/2}$ = *−11.68 ± 7.3 mV*, k = 29.0 ± 4.3 mV ($[Na^+]_i$ = 90 mM). Points shown and parameter estimates are given as the mean ± SEM (n = 6).

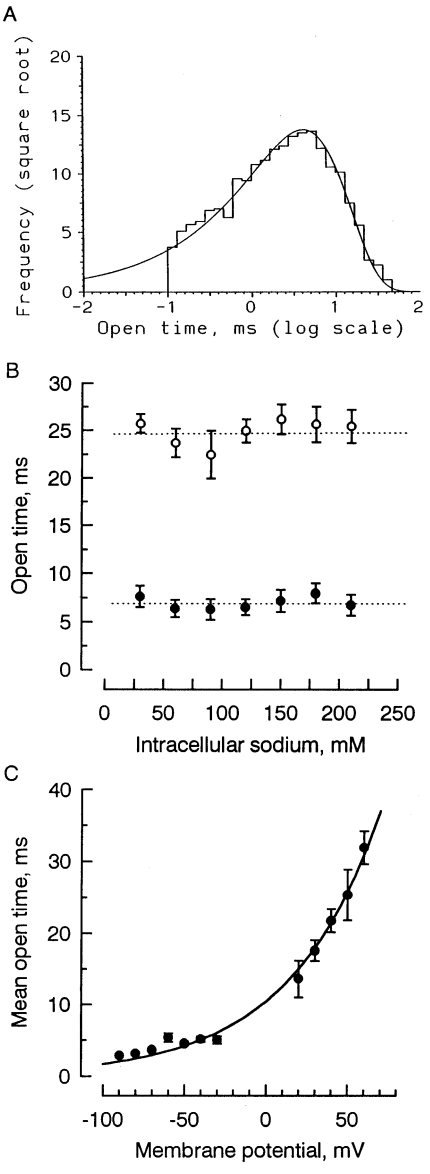

Fig. 5. (*A*) Distribution of open times of a single Na^+-activated channel (1975 openings). The distribution was fitted with a single exponent function with time constant 4.09 msec $[Na^+]_i$, 90 mM. Membrane potential, −60 mV. (*B*) Mean time constant of open duration distribution as a function of Na^+ concentrations at −60 mV (●) and +40 mV (○). The dashed lines were drawn by hand. (*C*) Mean time constant of apparent open durations as a function of voltage. $[Na^+]_i$, 90 mM. The solid lines through the data points were drawn according to the Eq. (5) in the text with parameters of $\tau_{o,\,o}$ = 10.51 msec and z = 0.45. Points shown are the mean ± SEM of the results from five different patches.

presumedly reflecting voltage dependency of rate constant(s) of Na^+ binding.

Dependence of Channel Kinetics on $[Na^+]_i$ and Voltage

Distribution of Open Time

The distribution of the apparent open times at −60 mV and 90 mM Na^+ could be fitted by a single-exponential function with time constant of 4.09 msec (Fig. 5*A*). This relationship held from 30 to 210 mM Na^+ and the open-time constant showed no considerable dependence on $[Na^+]_i$ (Fig. 5*B*). Average time constant over all $[Na^+]_i$ tested was 6.37 ± 0.43 (SEM) msec. At +40 mV, the distribution of apparent open times could still be fitted by a single-exponential function, but the open time constant increased to 23.72 ± 0.93 (SEM) msec (*data not shown*). Overall, the open time constant increased from 2.91 ± 0.04 (SEM) msec at −90 mV to 31.93 ± 2.29 (SEM) msec at +60 mV (Fig. 5*C*). The solid line through the data points in Fig. 5*C* is drawn according to the following equation:

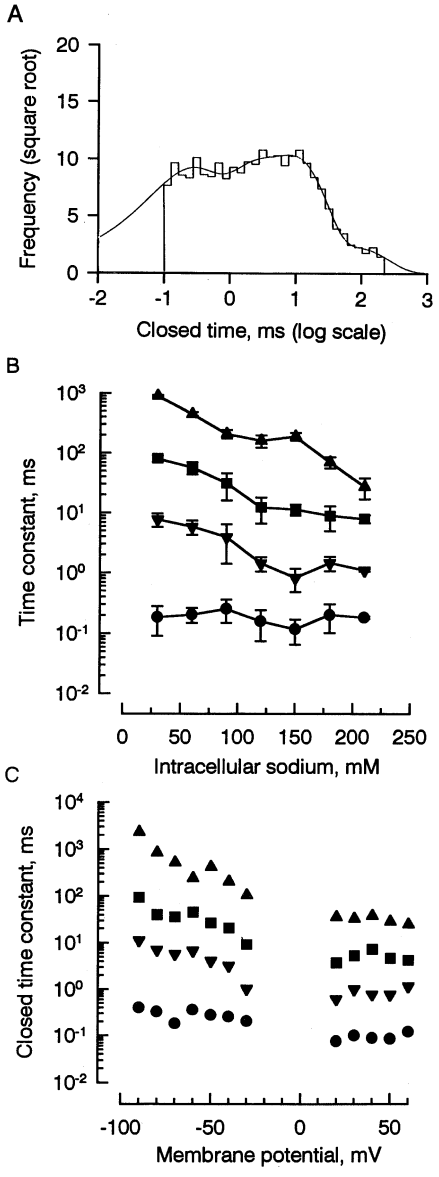

Fig. 6. Distribution of all closed times longer than 50 μsec in duration (1975 closing events). The distribution was fitted with the sum of four exponential components with parameters of (mean time constant (relative area)): 0.20 msec (28%), 1.46 msec (22%), 8.92 msec (48%), 69.9 msec (2%). Membrane potential, −60 mV. $[Na^+]_i$, 180 mM. (*B*) Relationship between the mean time constants of the distribution of all closed times and Na^+ concentration. (*C*) Mean time constants of all closed time distribution as a function of membrane potential. $[Na^+]_i$, 90 mM. In *B* and *C* the time constants are shown as the mean ± SEM (n = 5) ●, ▼, ■ and ▲ refer to the first, second, third and fourth components of all closed time distributions, respectively. The records were low-pass filtered at 2 kHz (−3 dB).

$$T_o = T_{o,o} \exp(zFV/RT), \quad (5)$$

where $T_{o,o}$ is the value of T_o at 0 mV, z is the valence of the gating charge that moves across the membrane potential drop V during channel activation, T is the absolute temperature. F and R are the usual physical constants. The fit yielded the parameters of $T_{o,o}$ = 10.51 msec and z = 0.45

Distributions of Closed Times

The closed time durations were dramatically decreased by membrane potential depolarization and increased $[Na^+]_i$ (Fig. 2*A*, and 3). the distribution of all closed time durations at 180 mM Na^+ and −60 mV could be fitted by the sum of the four exponential components with parameters (mean time constant (relative area)) of: $T1$ = 0.20 msec (28%), T_2 = 1.46 msec (22%), T_3 = 8.92% (48%) and T_4 = 69.9 msec (2%) (Fig. 6*A*). Due to the low-pass filtering properties of the recording system (2–4 kHz) and the finite duration of current traces (30–60 sec) used to compile the closed-time distribution, some of the very short-lived and long-lived closed time durations might be underrepresented in the distribution.

Only the three longer time constants decreased with $[Na^+]_i$ (30 to 210 mM) (Fig. 6*B*). There was no clear indication that the relative areas of all four time constants were dependent on $[Na^+]_i$ (*data not shown*). Five patches had closed time distribution parameters (mean ± (SEM) (relative area)) of: T_1 = 0.19 ± 0.09 msec (27 ± 5%), T_2 = 7.76 ± 2.00 msec (24 ± 5%), T_3 = 80.8 ± 10.4 msec (44 ± 5%), T_4 = 895.6 ± 23.1 msec (5 ± 3%) at 30 mM Na^+ and T_1 = 0.18 ± 0.01 msec (23 ± 5%), T_2 = 1.09 ± 0.05 msec (22 ± 5%), T_3 = 7.94 ± 1.24 msec (55 ± 2%), T_4 = 27.2 ± 10.1 msec (3 ± 1%) at 210 mM Na^+. The distribution mean decreased from 246.1 at 30 mM Na^+ to 9.1 msec at 210 mM Na^+.

All four time constants of the closed time distribution decreased as the membrane potential was increased from −90 to +60 mV, while the $[Na^+]_i$ was held at 90 mM (Fig. 6*C*), although the relative areas in the distribution did not vary (*data not shown*). Five patches had closed time distribution parameters (mean ± SEM (relative area)) of: T_1 = 0.40 ± 0.05 msec (53 ± 4%), T_2 = 11.44 ± 0.40 msec (25 ± 6%), T_3 = 94.0 ± 8.7 msec (21 ± 3%), T_4 = 2.31 ± 0.05 msec (2 ± 3%) at −90 mV and T_1 = 0.12 ± 0.02 msec (58 ± 6%), T_2 = 1.17 ± 0.30 msec (24 ± 7%), T_3 = 4.27 ± 0.74 msec (19 ± 4%), T_4 = 25.14 ± 6.4 msec (2 ± 3%) at +60 mV mM. The distribution mean decreased from 604.3 at −90 mV to 7.7 msec at +60 mV.

Burst Duration

Unlike the distributions of the open and the closed time durations, the distribution of the burst durations is relatively insensitive to the filtering properties of the recording system (Colquhoun & Sigworth, 1995). The distribution of the burst durations (critical time, 0.42 msec) at −60 mV and 150 mM Na^+ could be fitted with a single-exponential function with mean time constant of 7.87

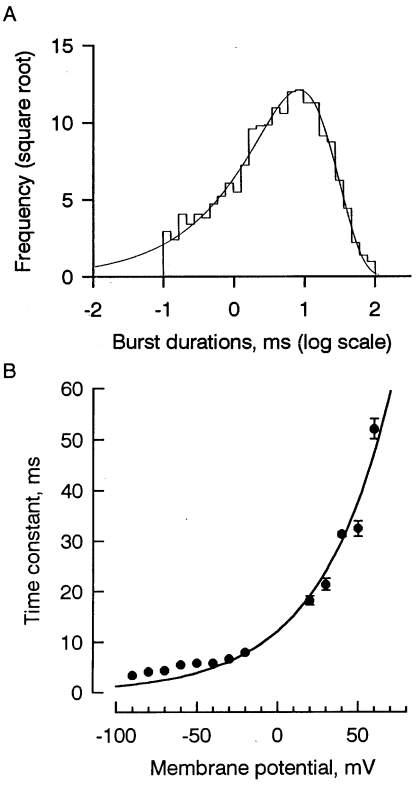

Fig. 7. (*A*) Distribution of burst durations (1718 bursts). The critical time t_c was set 0.42 msec. The distribution was fitted with a single-exponential function with mean time constant of 7.87 msec (*B*) relationship between the mean time constant of the burst duration distributions and the membrane potential. Points shown are the mean ± SEM of the results from five different patches. The solid line was drawn according to the Eq. (5) in the text with parameters of $T_{b,o} = 12.22$ msec and $z = 0.57$. $[Na^+]_i$, 210 mM.

msec (Fig. 7*A*). As shown by Colquhoun and Hawkes (1982), although theoretically the number of exponential components in the distribution of burst durations should equal the sum of the number of open and closed states within the burst, in many cases the burst duration distribution could be fitted by a single exponential function due to the inability to resolve short-lived closed periods within burst. Burst duration was not affected by change in $[Na^+]_i$ (*data not shown*), but when the membrane potential was changed from −60 to +40 mV, the burst duration increased from 7.26 ± 0.26 (SEM) msec to 31.32 ± 0.59 (SEM) msec ($n = 5$) (Fig. 7*B*). The solid line in Fig. 7*B* is the fit of Eq. (5) to the data points with parameters of $T_{b,o} = 12.22$ msec and $z = 0.57$.

Relative Permeabilities of the Na^+-activated Channel to Na^+ and Cl^-

Current through single Na^+-activated channels in patches excised from the plasma membrane of the soma of cultured ORNs reversed sign near zero (+0.1 ± 0.3 mV (SEM; $n = 10$) in symmetrical NaCl (210 mM). Changing the Cl^- concentration on the cytoplasmic side of the patch to approximately 1/20 of its normal value by substituting with sodium sulfate did not shift the reversal potential of the single-channel. Under these conditions ($[Cl^-]_o$, 210 mM; $[Cl^-]_i$, 12 mM), the single-channel current continued to reverse near zero (+1.7 ± 0.3 mV (SEM; $n = 3$) (Fig. 8*A*), suggesting that the channel was significantly more permeable to Na^+ than to Cl^-. The Goldmann-Hodgkin-Katz equation:

$$E_r = (RT/F)ln\{(P_{Na}[Na^+]_o + P_{Cl}[Cl^-]_i)/ (P_{Na}[Na^+]_i + P_{Cl}[Cl^-]_o)\}, \quad (6)$$

was used to estimate the relative permeability ratio to these two ions, even though it assumes independent movement of ions and a constant electrical field and may not strictly apply. This approach estimated the permeability of Cl^- relative to Na^+ (P_{Cl}/P_{Na}) as 0.06.

The reversal potential of the Na^+-activated single-channel current depended on $[Na^+]_i$. Figure 8*B* illustrates the relation between $[Na^+]_i$ and the reversal potential when the Cl^- concentration was kept constant. The data points are very close to the relationship predicted by the Nernst equation for Na^+ (solid line, Fig. 8*B*), consistent with the idea that the channel is highly permeable to Na^+.

Relative Permeabilities of the Na^+-activated Channel to Alkali Metal Cations

The reversal potential of single Na^+-activated channels changed when the cytoplasmic side of the membrane was bathed with solutions containing 210 mM Na^+, compared to when the bath contained 90 mM Na^+ +120 mM of one of the following alkali metal cations, Li^+, K^+, Cs^+, and Rb^+ (Fig. 8*C*). The reversal potential determined under these ionic conditions was +0.1 ± 0.3 (SEM; $n = 10$) mV for Na^+, −1.6 ± 0.4 (SEM; $n = 3$) mV for Li^+, +11.4 ± 0.6 (SEM; $n = 3$) mV for Rb^+ and +15.4 ± 1.4 (SEM; $n = 5$) mV for Cs^+, respectively. The permeability of these alkali metal cations relative to that of Na^+ (P_X/P_{Na}), calculated from the shift in reversal potential by using Eq. (1), was Li^+ (1.11) > Na^+ (1.0) > K^+ (0.54) > Rb^+ (0.36) > Cs^+ (0.20).

Conductance of the Na^+-activated Channel Under Physiological Extracellular Ionic Conditions

Na^+-gated channel activity can be evoked with *Panulirus* saline in the pipette, even though *Panulirus* saline contains high concentrations of both $MgCl_2$ (9.8 mM) and $CaCl_2$ (13.6 mM) (Fig. 9*A*). This result is in contrast to

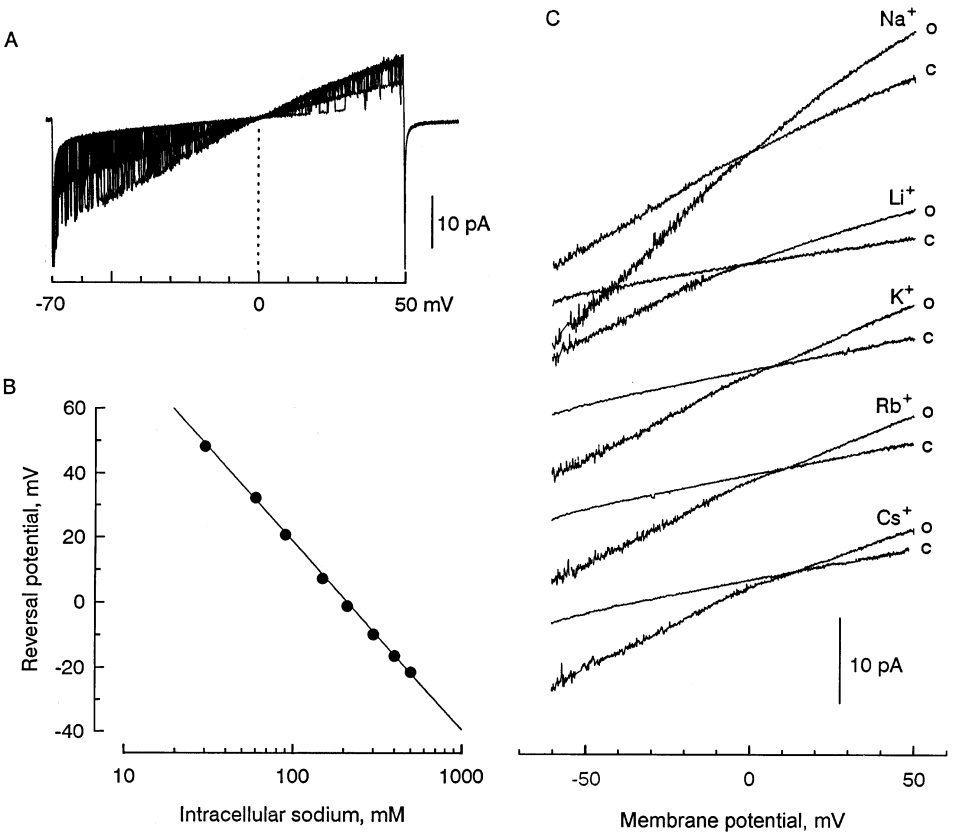

Fig. 8. (*A*) Current-voltage relationships of single-channel currents activated by intracellular Na^+. Twenty superimposed traces of a patch containing two Na^+-activated channels exposed to voltage ramp from −70 to +50 mV (300 msec). Pipette, standard pipette solution (Materials and Methods). Bath (in mM): 100 Na_2SO_4, 10 NaCl, 11 EGTA, 1 $CaCl_2$, 10 HEPES, and 696 glucose, pH 7.4 adjusted with Tris base. (*B*) Plot of the reversal potential as a function of $[Na^+]_i$. Points shown are the mean ± SEM of 5–7 trials. The solid line represents the calculated Nernst potential for sodium, and has a slope of 57 mV per 10-fold change in $[Na^+]_i$. Bath solution (in mM): 500 NaCl, 1 $CaCl_2$, 11 EGTA, and 10 HEPES, pH 7.4 adjusted with TRIS base. $[Na^+]_i$ changed by replacing the part of the NaCl by an equivalent concentration of choline-Cl and adjusting the osmolarity to 1014 mmol/kg with glucose. Pipette, standard pipette solution (Materials and Methods). (*C*) Current-voltage relationships of a single Na^+-activated channel with different permeant monovalent cations. Pipette, the standard pipette solution. Bath solution (in mM): 90 NaCl and 120 one of the following alkali metal chloride: NaCl, LiCl, KCl, RbCl, and CsCl. The value of reversal potential for the Na^+-activated channel current is a potential where the open channel current-voltage curve (o) intercepts the leakage current-voltage curve (*c*). The open Na^+-activated channel current reverses polarity at: −0.3 mV, NaCl (210 mM); −1.7 mV, LiCl (120 mM)/NaCl (90 mM); 7.0 mV, KCl (120 mM)/NaCl (90 mM); 11.2 mV, RbCl (120 mM)/NaCl (90 mM), and 14.0 mV, CsCl (120 mM)/NaCl (90 mM), respectively.

the effect of divalent cations on the cytoplasmic side of the membrane, which completely block the channel at 1 mM (Zhainazarov & Ache, 1995*a*). The estimated slope conductance of the channel under these conditions, however, was 25.7 ± 0.7 pS (SEM; $n = 5$) between −90 and −20 mV (Fig. 9*B*), suggesting that while the divalent cations did not block the channel completely from the extracellular side, the single-channel conductance was still decreased considerably from that obtained in the absence of extracellular divalents.

Blocking by Extracellular Divalent Cations of the Na^+-activated Channel

To study the blocking effect of divalent cations on the single-channel current, 10 mM of $MgCl_2$, $CaCl_2$, $BaCl_2$, $MnCl_2$, or $SrCl_2$ was included in the pipette solution. Under these conditions, the Na^+ current was considerably reduced in relative to that in the absence of divalent cations at every membrane potential from −100 to +100 mV. These effects are illustrated in Fig. 10*A* which shows the current-voltage relationships obtained in the absence of divalent cations (1) and in the presence of 10 mM Mg^{2+} (2) in the pipette solution. In the presence of 10 mM Mg^{2+} the current-voltage relationship shows a strong outward rectification in contrast to the slight inward rectification observed in the absence of divalent cations. The similar current-voltage relationships were observed for all tested divalent cations indicating that the blocking effect of these divalent cations is voltage-dependent. The ratio of the single-channel current in the presence of divalent cation relative to the current in its

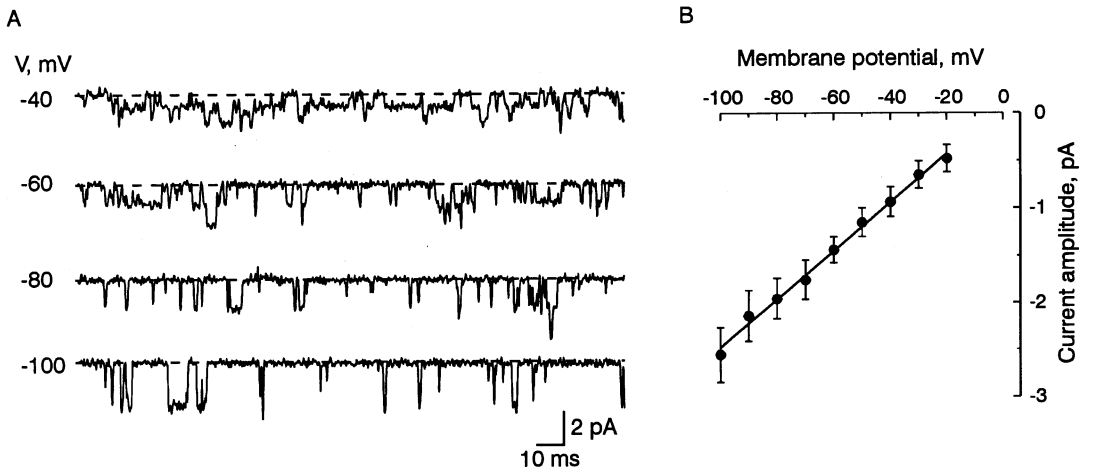

Fig. 9. Na^+-activated channel activity in the presence of high extracellular divalent ions. (*A*) Traces of activity at the membrane potentials indicated next to the traces. Pipette, *Panulirus* saline. Bath, 210 mM NaCl. This particular patch contained four Na^+-activated channels. (*B*) Plot of the current-voltage relation of the channel under these conditions. Each point is the mean (± SEM) of five different experiments. Slope conductance was 25.7 pS between −100 and −20 mV. Records low-pass filtered at 2 kHz (−3 dB). Channel openings are shown as downward deflections.

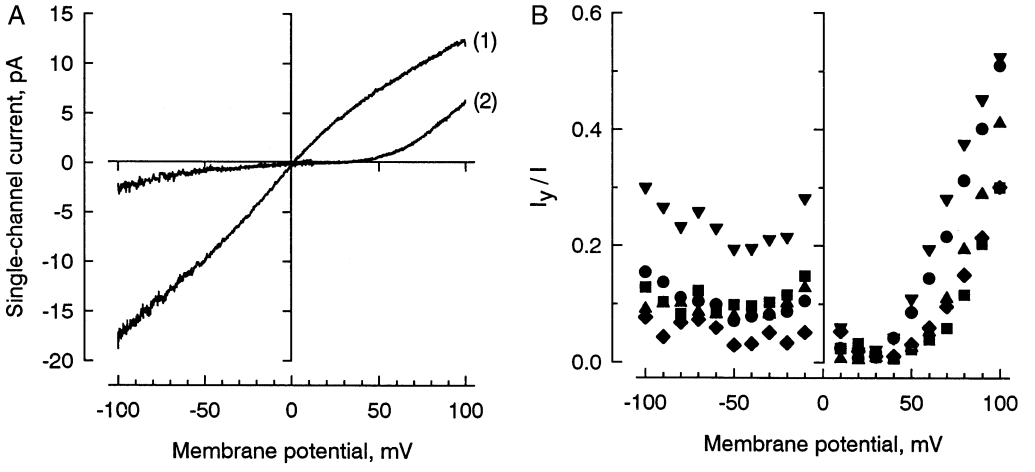

Fig. 10. The blocking effect of divalent cations on the Na^+-activated channel current. (*A*) Current-voltage relationship of the Na^+-activated channel obtained in the absence of divalent cations (1) and in the presence of 10 mM Mg^{2+} (2) in the pipette solution. (*B*) The voltage-dependence of the blocking effect of divalent cations. The ratio I_Y/I is plotted as a function of membrane potential for $MgCl_2$ (●), $CaCl_2$ (■), $BaCl_2$ (▼), $SrCl_2$ (▲), and $MnCl_2$ (♦). Pipette solution in the absence of divalent cations (in mM): 210 NaCl, 0.1 EGTA, 0.1 EDTA, 10 HEPES, 686 glucose, pH 7.4. Pipette solution in the presence of divalent cations (in mM): 190 NaCl, 10 Na acetate, 10 HEPES, 686 glucose and 10 of one of the following divalent cations: $MgCl_2$, $CaCl_2$, $BaCl_2$, $SrCl_2$, and $MnCl_2$. Bath, 210 mM NaCl.

absence as a function of membrane potential is shown in Fig. 10*B*. The sequence of blocking efficiency (I_Y/I) for divalent cations on the inward current at −60 mV was Mn^{2+} (0.06) > Ca^{2+} (0.08) > Sr^{2+} (0.09) > Mg^{2+} (0.10) > Ba^{2+} (0.23). If the divalent cation binding site is within the channel pore and the blocking divalent cation does not permeate through the channel, its blocking effect must obey the Woodhull equation (Woodhull, 1973):

$$I_Y/I = K_Y/\{K_Y + [Y]_o \exp(-2\delta FV/RT)\}, \quad (7)$$

where V is the membrane potential, R the gas constant, F the Faraday constant, T the absolute temperature, δ the electrical distance, $[Y]_o$ the extracellular concentration of the blocking divalent cation, K_Y the dissociation constant of the divalent cation-channel complex, I_Y and I the single-channel current in the presence and the absence of the divalent cation. The Woodhull equation predicts that the blocking effect of the divalent cation will increase steadily with negative membrane potential. But the data shown in Fig. 10*B* demonstrate that the blocking effect of all divalent cations is relieved at high negative potentials. The most plausible explanation for such a discrepancy is the permeation of the blocking divalent cations through

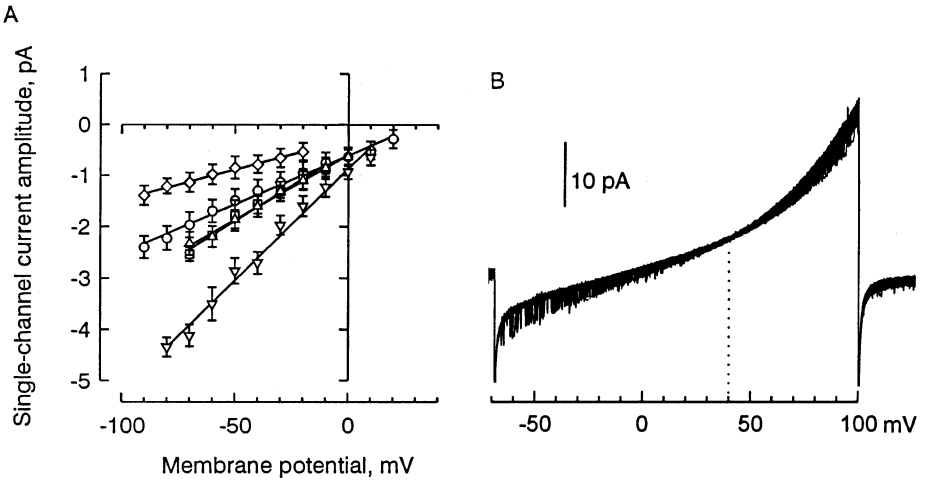

Fig. 11. Permeability of the Na^+-activated channel to divalent cations. (*A*) Plot of the single-channel current-voltage relations of Na^+-activated channels in the presence of extracellular Mg^{2+} (○), Ba^{2+} (▽), Ca^{2+} (□), Sr^{2+} (△), and Mn^{2+} (◇). Pipette solution (in mM): 10 HEPES and 105 mM chlorides of one of the following alkaline earth cations: $BaCl_2$, $CaCl_2$, $SrCl_2$, $MgCl_2$, and $MnCl_2$. Bath, 210 mM NaCl. Points are the mean ± SD of 4 different experiments. (*B*) Single-channel current traces evoked by a voltage ramps from −70 to 100 mV (450 msec). The trace is a superposition of 30 ramps. Before and after voltage ramps the membrane was voltage-clamped to 0 mV. Pipette, 105 mM $BaCl_2$. Bath, 210 mM NaCl.

the channel. In the following section we will show that divalent cations indeed permeate the Na^+-activated channel.

The Woodhull equation also predicts that the blockage by divalent cations should be relieved at positive potentials. At +60 mV divalent cations still block the channel with the blocking efficiency: Ca^{2+} (0.04) > Sr^{2+} (0.05) > Mn^{2+} (0.06) > Mg^{2+} (0.14) > Ba^{2+} (0.19). The blocking effect was present even at membrane potential of +100 mV (Fig. 10*B*). These results suggest that in addition to the voltage-dependent blockage divalent cations can also block the channel in a non-voltage-dependent manner by binding to a site at the extracellular side of the channel which is not within the electric field across the membrane.

Free Ca^{2+} concentration in the standard pipette solution was typically buffered at 10 nM with high concentration of EGTA (11 mM). When lower concentrations of EGTA (0.1–2 mM) were used, the amplitude of single-channel current increased at all tested potentials relative to those recorded with high concentration of the buffer (Fig. 2*D* and 10*A; see also* Fig. 13*D*). But the current-voltage relationship of open channel current again showed slight inward rectification at positive potentials (Fig. 10*A*). We did not also observe any difference in the dwell-time characteristics of the channel when low concentrations of the calcium buffer were used. The slope conductance of the channel was 169.8 ± 5.4 (SD) pS ($n = 3$) between −90 and 10 mV, with reversal potential 0.6 ± 0.4 (SD) mV ($n = 3$). It seems that Ca buffer at high concentrations decreases the amplitude of single-channel current without affecting appreciably other parameters. But we did not investigate this effect in detail.

Divalent Cation Permeation Through the Na^+-activated Channel

Permeation of divalent cations through the Na^+-activated channel currents were determined with 105 mM chloride and one of the following alkaline earth cations: $BaCl_2$, $MgCl_2$, $CaCl_2$, $SrCl_2$ or $MnCl_2$ in the pipette. The inward current carried at −60 mV by the divalent cations was −3.50 ± 0.31 pA (SD) for Ba^{2+}, −2.19 ± 0.06 pA for Ca^{2+}, −2.17 ± 0.20 pA for Sr^{2+}, −1.69 ± 0.22 pA for Mg^{2+}, and −0.97 ± 0.10 pA for Mn^{2+}. The slope conductance calculated in the range of membrane potential from −100 to +20 mV was 43.4 ± 0.2 pS (SEM) for Ba^{2+}, 27.7 ± 0.1 pS for Ca^{2+}, 25.2 ± 0.7 pS for Sr^{2+}, 19.1 ± 0.6 pS for Mg^{2+}, and 11.9 ± 0.4 pS for Mn^{2+} (Fig. 11*A*). The ratio of the inward current carried by the divalent cations to that carried by Na^+ (G_Y/G_{Na}, conductance ratio) at −60 mV gave the following selectivity sequence: Na^+ (1.0) > Ba^{2+} (0.57) > Ca^{2+} (0.36) > Sr^{2+} (0.35) > Mg^{2+} (0.27) > Mn^{2+} (0.18).

To determine permeability of alkaline metal cations relative to that of Na^+ (P_Y/P_{Na}) reversal potentials were measured under above described bi-ionic conditions by applying a voltage ramp from −70 +100 mV in duration of 450 msec (Fig. 11*B*). The current through the channel reversed at +39.5 ± 0.2 mV (SEM; $n = 4$) in the presence of extracellular 105 mM $BaCl_2$ (210 mM NaCl intracellular). Extracellular 105 mM $CaCl_2$ shifted the reversal potential to +53.6 ± 0.7 mV (SEM; $n = 3$) mV, while 105 mM $MgCl_2$ shifted it to +51.8 ± 0.7 mV (SEM; $n = 4$) and

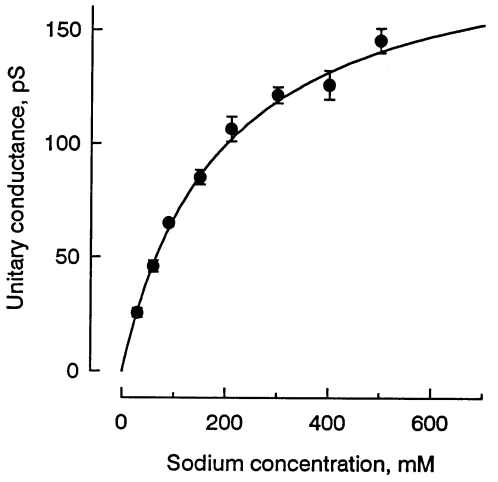

Fig. 12. Plot of the dependence of the slope conductance of the Na^+-activated channel on the $[Na^+]_i$. Membrane potential, + 50 mV. Patch pipette, 210 mM NaCl. Bath, NaCl + choline chloride to provide the sodium concentration indicated on the abscissa. Points are the mean ± SEM of four experiments. The solid line through the data is drawn according to the Michaelis-Menten equation $\gamma = Y_{max}/(1 + K_D/[Na^+]_i)$, where Y is the unitary conductance, Y_{max} is the value of Y at saturating concentrations of Na^+, and K_D is the apparent dissociation constant. The best fit to the data was obtained with parameters of Y_{max} = 193.3 pS and K_D = 187.9 mM.

105 mM $MnCl_2$ shifted it to +41.1 ± 0.5 mV (SEM; n = 5). The permeability ratio sequence relative to Na^+ (P_Y/P_{Na}), calculated using Eq. (2), was Ca^{2+} (39.0) > Mg^{2+} (34.1) > Mn^{2+} (15.5) > Ba^{2+} (13.8) > Na^+ (1.0), indicating that the channel is considerably more permeable to divalent cations than to Na^+. This sequence differs appreciably from the selectivity sequence (G_Y/G_{Na}) based on conductance measurements.

Dependence of the Channel Conductance on the Permeant Ion Concentration

The conductance of the channel increases as a nonlinear function of the concentration of the permeant ion (Na^+) on the cytoplasmic side of membrane (Fig. 12). The observed concentration-response function could be fit by the Michaelis-Menten equation with an apparent dissociation constant for Na^+ (K_D) of 187.9 mM and a maximal conductance (Y_{max}) of 193.3 pS (solid line, Fig. 12). Such a nonlinear relation between the channel conductance and the permeant ion concentration suggests that ion fluxes through the channel do not obey the concept of independent movement of ions. It is believed that saturation of ion fluxes takes place when the binding-unbinding site(s) of permeation inside the channel pore become rate limiting (Hille, 1992).

Mole Fraction Behavior of the Single Channel Current Through the Na^+-activated Channel

To determine how many ions can occupy simultaneously the permeation pathway of channel, i.e., the mole-fraction behavior of the current (Hille, 1992), the conductance and the reversal potential of the single-channel current were measured in the presence of intracellular solutions consisting of varying mixtures of Na^+ and either Cs^+ (Fig. 13*A*) or Li^+ (Fig. 13*B*). The single-channel conductance and the reversal potential of the current in both sets of conditions were monotonic functions of the mole fraction $[X^+]_i/([Na^+]_i + [X^+]_i)$, suggesting that the channel is a single-ion pore with a simple saturating binding site in the absence of divalent cations.

Many Ca channels typically reveal an anomalous mole-fraction behavior of current, a channel passes lower current in mixture of two divalent cations than in either divalent cations alone (Hille, 1992). As the Na^+-activated channel shows very high relative permeability to Ca^{2+} (P_{Ca}/P_{Na} = 39.0), it was interesting to look into whether the channel shows an anomalous mole-fraction behavior when the single-channel current is carried exclusively by divalent cations. We measured the single-channel current at −60 mV and the reversal potential of the single-channel current when the pipette consisted of varying mixture of Ca^{2+} and Ba^{2+} ($[Ca^{2+}]_o + [Ba^{2+}]_o$ = 105 mM) (Fig. 13*C*). The single-channel current and its reversal potential indeed went through a minimum and maximum, respectively, when extracellular Ba^{2+} was gradually replaced with Ca^{2+} (Fig. 13*C*). This result suggests that the channel behaves itself as a multi-ion pore when the current is carried exclusively by divalent cations.

All the inward current through the channel is carried by Na^+ at low Ca^{2+} concentrations (≤10 nM). As $[Ca^{2+}]_o$ is increased, the inward current gradually decreases until it reaches a minimum at 1 mM extracellular Ca^{2+} (Fig. 13*D*). Ca^{2+} decreases the inward current carried by Na^+ presumedly by binding to a blocking site inside pore. At Ca^{2+} concentrations above 1 mM the inward current raises again, but now carried by Ca^{2+}. Similar effects observed in voltage-activated Ca channels have been explained as an anomalous mole-fraction effect in a multi-ion (Almers & McCleskey, 1984; Hille, 1992).

Discussion

Channel Conductance

The lobster channel, like the previously reported Na^+-activated nonselective cation channels (Stuenkel et al., 1990; Nouailhetas et al., 1995), appears to have a single main conductance level. This is in contrast to Na^+-

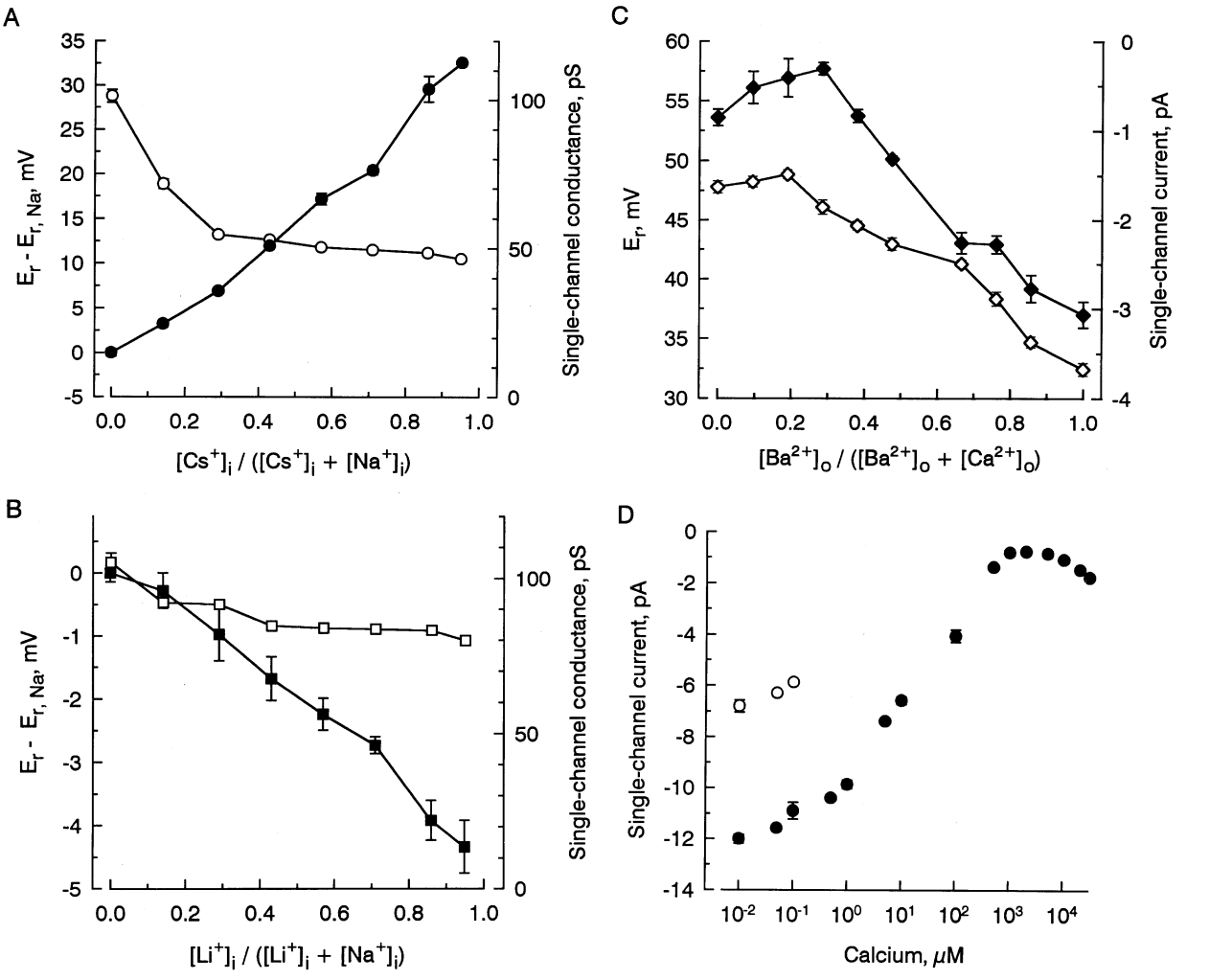

Fig. 13. Mole-fraction behavior of the single-channel current. (*A* and *B*) Mole-fraction dependence of the conductance (open symbols) and the reversal potential (closed symbols) of the single-channel current the Na^+-activated channel with mixtures of Na^+ and Cs^+ (circles in *A*), and Na^+ and Li^+ (squares in *B*) to obtain the concentration ratio indicated on the abscissa. $[Na^+]_i + [X^+]_i$ = 210 mM. Pipette, $[Na^+]_o$ = 210 mM. Points shown are the mean ± SEM of four experiments. (*C*) The single-channel current (◇) measured at −60 mV and the reversal potential (♦) of the current through the Na^+-activated channel as a function of mole-fraction in mixture of Ba^{2+} and Ca^{2+}. $[Ba^{2+}]_o + [Ca^{2+}]_o$ = 105 mM. Bath, $[Na^+]_i$ = 210 mM. (*D*) Dependence of the current through the Na^+-activated channel recorded at −60 mV as $[Ca^{2+}]_o$ (●; no added Mg^{2+}) is varied. Points shown are the mean ± SEM of three experiments. $[Na^+]_i = [Na^+]_o$ = 210 mM. $[Ca^{2+}]_i$ = 10 nM. In *D* open (closed) circle points represent the single-channel current at −60 mV recorded when $[Ca^{2+}]$ was buffered with high (low) concentration EGTA. $[EGTA]^{high}$ = 11 mM. $[EGTA]^{low} \leqslant 2$ mM.

activated K^+ channels, which exhibit frequent openings to variety of subconductance open states (*see* review Dryer, 1994). The conductance of the lobster channel (104 pS) is relatively close to that of the Na^+-activated cation channel from crab peptidergic nerve terminals (79 pS; Stuenkel et al., 1990), but differs from that of the Na^+-sensitive cation channel in mammalian intestinal myocytes (12 pS; Nouailhetas et al., 1995). The conductance of the latter channel was determined in extracellular solution containing 1 mM Mg^{2+}, however, so the reported value might reflect Mg^{2+} block, since bathing the extracellular side of the lobster channel with high divalents (*Panulirus* saline), reduced the conductance of the lobster channel to 25.7 pS.

Effect of Na^+ Concentration and Voltage on Channel Open Probability

The lobster channel is strongly dependent on $[Na^+]_i$ and the sigmoidal nature of the relationship between P_o and $[Na^+]_i$ with a Hill coefficient > 3 indicates that binding of at least four Na^+ is necessary to activate the channel. No quantitative data are available on the Na^+ concentration dependency of P_o for other Na^+-activated nonselective cation channels, but the P_o of Na^+-activated K^+ channels is also strongly dependent on $[Na^+]_i$ with $K_{1/2}$ ranging from 7.3 to 80 mM and Hill coefficients from 2.7 to 4.6 (*see review* Dryer, 1994).

The voltage dependency of the gating of the lobster

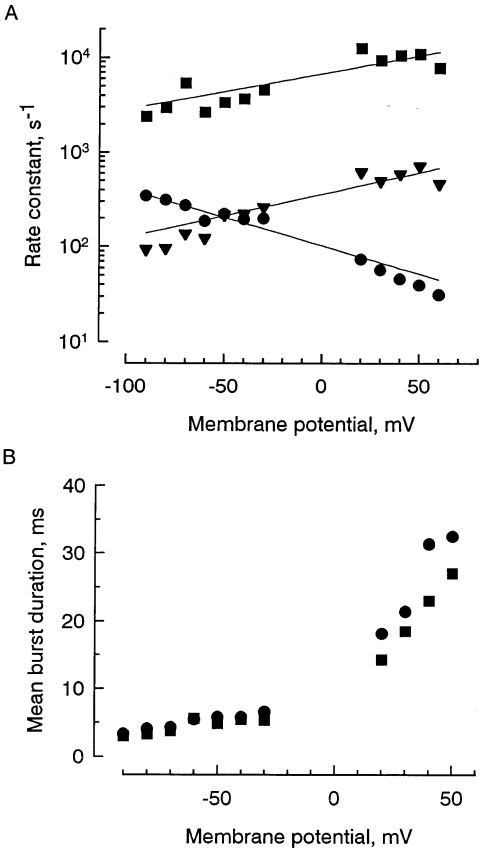

Fig. 14. (*A*) Semilogarithmic plot of rate constants α (●), β (▼), and k_{-4} (■) as a function of the membrane potential. The solid lines were drawn through points according to the Eq. (5) with parameters of: α_o = 102.2 s^{-1} (z = −0.36), β_0 = 357.4 sec^{-1} (z = 0.27), and $k_{-4,\,o}$ = 6765 sec^{-1} (z = 0.22). (*B*) Mean burst duration as a function of the membrane potential. The points (●) and (▼) refers to the value of the mean burst duration observed in the experiment and predicted from the kinetic model, respectively.

channel by Na^+ (Fig. 2*A* and 4) can be explained by a combination of two distinct effects. First effect, the rate constants of Na^+ binding is voltage-dependent. Three experimental observations implicate such a mechanism for the lobster channel: (*a*) although the Hill coefficient was not affected by membrane depolarization, $K_{1/2}$ was voltage-dependent; it is almost two times less at +40 mV than −60 mV; (*b*) at nonsaturating $[Na^+]_i$ (90 mM), when the channel is not fully ligand-bound, the voltage dependency of the channel P_o shifted along the voltage axis without changing the slope (Fig. 4*B*); (*c*) all four time constants in the closed time distribution are decreased by membrane depolarization (Fig. 6*C*), and at least some of these should be related to the rate constants of the ligand-binding stages. Second effect, the transmembrane electrical field presumably can move charged components of fully bound channels to change the gating of the channel. This mechanism is also implicated in activation of the lobster channel since the open probability at saturating $[Na^+]_i$ increased e-fold per 37 mV on membrane depolarization (Fig. 4*B*), suggesting that the rate constants of the transitions of the fully ligand-bound channel between open and closed states solely depend on membrane potential. The voltage dependence of the rate constants of Na^+ binding could be interpreted in two different ways. If ligand-binding sites are within the transmembrane electrical field, presumably in the channel pore region, soluble ions such as Na^+ would have to move through the transmembrane electrical field in order to reach those binding sites, which would be expected to influence the rate constants of Na^+ binding. Alternatively, the Na^+ binding site is not in the electric field (not in the channel pore), but the electric field acts on the channel to influence the affinity and/or availability of the site. The latter interpretation may be more appropriate to the lobster channel since binding of four Na^+ to the channel is required to activate the channel. If Na^+ binding sites are within the channel pore, the channel should demonstrate multiple occupancy for monovalent cations, yet in the absence of divalent cations the channel behaves as a single-ion pore (Fig. 14*A* and *B*). The Na^+-sensitive cation channel from guinea pig intestinal myocytes also increases its open probability e-fold per 29 mV (Nouailhetas et al., 1994), although the P_o of the Na^+-activated cation channel from crab peptidergic terminals (Stuenkel et al., 1990) is largely independent of membrane potential. The voltage dependence of gating of Na^+-activated K^+ channels is similarly variable in that those from chick sensory ganglion neurons (Haimann et al., 1990), rat olfactory bulb neurons (Egan et al., 1992*a*), and *Xenopus* spinal neurons (Dale, 1993) show varying degrees of increased P_o with membrane depolarization, while others from guinea pig ventricular myocytes (Kameyama et al., 1984) and chick midbrain neurons (Dryer et al., 1989) are voltage-independent.

The significance of having such a dual dependency of the open probability of the lobster channel on both ligand concentration and membrane potential is unclear. Presumably, if Na^+-activated cation channels were activated by Na^+ influx through nonselective cation channels activated by neurotransmitters, the increased open probability at positive potentials would facilitate activation of the channel. Such a dual dependency of the open probability on ligand (Ca^{2+}) concentration and membrane potential also occurs in the large Ca^{2+}-activated K channel (Gorman & Thomas, 1980; Pallota, Magleby & Barrett, 1981; Moczydlowski & Latorre, 1983), suggesting the functional significance may be of general utility.

Effect of Na^+ Concentration on Channel Kinetics

We interpret the bursting behavior of the lobster channel (Fig. 2A and 3) as fluctuation of the fully ligand-bound

channel between open and closed stages before losing one of four bound Na^+ and suggest that the rate constants of these transitions are concentration-independent for the following reasons. First, the distribution of the apparent open times could be fit by a single-exponential function, indicating that the channel has a single open state (Fig. 5*A*). The open time constant was independent of $[Na^+]_i$. Second, the shortest time constants in the closed time distribution did not vary with $[Na^+]_i$ (Fig. 6*B*), indicating that the lifetime of one of the closed states, which presumably corresponds to brief closings within bursts, is independent of $[Na^+]_i$. Third, since increased $[Na^+]_i$ did not affect burst duration, it seems that channel transitions within bursts are not associated with Na^+ binding. The distributions of closed and open time durations within bursts were fit by single-exponential functions with time constants close to the shortest time constant observed. In contrast to openings and closings within bursts, the three longer time constants in the closed time distribution, which presumably correspond to closings between bursts, decreased with increasing of $[Na^+]_i$ (Fig. 6*B*). So the increase in the P_o with increased $[Na^+]_i$ was mainly due to decrease of the average closed time duration between bursts.

This interpretation could be at least qualitatively illustrated in the frame of the following minimal kinetic model of channel activation based on the kinetic model first suggested for activation of the nicotinic acetylcholine receptor channel (del Castillo & Katz, 1957; Colquhoun & Sakmann, 1981, 1985):

$$C_0 \underset{k_{-1}}{\overset{k_1[Na^+]}{\rightleftharpoons}} C_1 \underset{k_{-2}}{\overset{k_2[Na^+]}{\rightleftharpoons}} C_2 \underset{k_{-3}}{\overset{k_3[Na^+]}{\rightleftharpoons}} C_3 \underset{k_{-4}}{\overset{k_4[Na^+]}{\rightleftharpoons}} C_4 \underset{\alpha}{\overset{\beta}{\rightleftharpoons}} O$$

where C_i represents the closed state of the channel with i number of Na^+ bound, O the open state of the channel. A similar kinetic model of channel activation has also been used to describe the gating of single cyclic nucleotide-activated channels in retinal rods and cones (Karpen et al., 1988; Haynes & Yau, 1990).

The five closed states in the model reflect our observation that binding of four Na^+ to the channel is required to activate the channel. Bursts of openings observed over a wide range of $[Na^+]_i$ (Fig. 3) would be represented in this model by multiple rapid transitions of the channel between C_4 and O states before losing one of four Na^+ bound and entering the state C_3. In this kinetic model, the mean open time, T_o, the mean intraburst closed time, T_c, the mean burst duration, T_b, are related to the rate constants α, β, and k_{-4} through the following equations (Colquhoun & Hawkes, 1995):

$$T_o = 1/\alpha \tag{8}$$

$$T_c = 1/(k_{-4} + \beta) \tag{9}$$

$$T_b = [(k_{-4} + \beta)^2 + \beta\alpha]/k_{-4}\alpha(k_{-4} + \beta) \tag{10}$$

The models predict that T_o, T_c, and T_b do not depend on $[Na^+]_i$, in good agreement with the experimental observations. At saturating $[Na^+]_i$ the channel would behave as a two-state channel fluctuating between the states C_4 and O, with the channel P_o given by the equation:

$$P_o = \beta/(\alpha + \beta) \tag{11}$$

Comparative data on channel kinetics are not available for other known Na^+-activated nonselective cation channels, but Na^+-activated K^+ channels from guinea-pig ventricular myocytes (Kameyama et al., 1984) and chick midbrain ganglion neurons (Dryer et al., 1989) also open in bursts separated by closures of short durations, while adjacent bursts are separated by long closed intervals, as in the lobster channel. In Na^+-activated K^+ channels from guinea-pig ventricular myocytes, increase in $[Na^+]_i$ affects the time constants of the open time distribution, and the fast and slow components of the closed time distribution, but the predominant effect was to decrease the interval between bursts (Kameyama et al., 1984), similar to the kinetics of the lobster channel.

Effect of Voltage on Channel Kinetics

Our results indicate that the increase in the channel P_o with membrane depolarization was mediated by an increase of both the mean channel open time and burst duration and a decrease of both the averaged closed time duration between bursts and the mean duration of the brief closings within bursts. Such dependence of the dwell-time characteristics on membrane polarity is consistent with the idea discussed above that the ligand-binding sites of the channel are within the transmembrane electrical field and the fully ligand-bound channel undergoes voltage-dependent conformation change. In terms of the minimal kinetic model, it would require voltage-dependence of the rate constants of all channel transitions. Using the Eq. (8), (9), (10), (11) and the value of open probability measured at saturating $[Na^+]_i$ (Fig. 4*B*), we evaluated some of the rate constants, namely, α, β, and k_{-4} in the kinetic model. At −60 mV, α = 185.7 sec^{-1}, β = 123.3 sec^{-1}, and k_4 = 2646.8 sec^{-1}. Figure 14*A* shows the estimated values of these three rate constants over range of membrane potential. The rate constants β and k_{-4} increased, but α decreased with membrane depolarization (Fig. 14*A*).

We tried to evaluate the kinetic model by calculating the mean burst duration at different membrane potentials with the use of both Eq. (10) and the values of the rate constants and comparing it with the mean burst duration observed in the experiments (Fig. 7*B*). The results of such an evaluation are illustrated in Fig. 14*B*. Although

the predicted values are slightly less than observed at positive potentials, the model makes relatively good prediction of the mean burst duration. We conclude, therefore, that the kinetic model describes the gating of Na^+-activated channel with a reasonable degree of certainty.

Conduction Properties

The conduction properties of the Na^+-activated channels from lobster ORNs are similar to those of other Na^+-activated (or -sensitive) cation channels in being highly selective for cations over anions, $P_{cl}/P_{Na} = 0.06$ (lobster) *vs.* 0.07 (guinea pig intestinal myocytes; Nouailhetas et al., 1994). The lobster channel appears to differ, however, in its permeability sequence. The permeability sequence of the lobster channel for alkali monovalent cations ($Li^+ > Na^+ > K^+ > Rb^+ > Cs^+$) corresponds to the Eisenman sequence XI for strong field and strength site (Hille, 1992), but differs from that of the Na^+-sensitive cation channel of guinea pig ileum myocytes ($Li^+ > Na^+ = K^+$) in that the latter has equal permeability Na^+ and K^+ (Nouailhetas et al., 1994). The Na^+-activated cation channel from crab nerve peptidergic terminals also has equal permeability to Na^+ and K^+ ($P_K/P_{Na} = 0.94$), and is impermeable to Cs^+ as well (Stuenkel et al., 1990), again unlike the lobster channel ($P_K/P_{Na} = 0.54$).

It appears that extracellular divalent cations also permeate the lobster channel while they block partially the channel by reducing its conductance to Na ions. The sequence of blocking potency of divalent cations on the inward Na^+ current at −60 mV was $Mn^{2+} > Ca^{2+} > Sr^{2+} > Mg^{2+} > Ba^{2+}$. The selectivity sequence of the lobster channel determined for divalent cations from the ratio of the currents carried by divalent cations over one carried by Na^+ (conductance ratio) was Na^+ (1.0) > Ba^{2+} (0.57) > Ca^{2+} (0.36) ⩾ Sr^{2+} (0.35) > Mg^{2+} (0.27) > Mn^{2+} (0.18). This sequence differs significantly from that determined from reversal potential measurements (permeability ratio): Ca^{2+} (39.0) > Mg^{2+} (34.1) > Mn^{2+} (15.5) > Ba^{2+} (13.8) > Na^+ (1.0). Conductance and permeability ratios are two different ways of determining selectivity and they do not always give similar sequences (Hille, 1992). The difference between these two selectivity sequences for divalent cations might be the result of partial saturation or blockage of the channel by the permeant ions in conductance measurement experiments (Hille, 1992). Indeed, the conductance of the Na^+-activated channel depended on the permeant ion concentration, and its concentration dependence followed the Michaelis-Menten equation (Fig. 6). It is interesting to note that the Na^+-activated channel behaves as a single-ion pore with simple saturating binding site when the current is exclusively carried by monovalent cations, but in the presence of divalent cations at millimolar concentrations it becomes a multi-ion pore channel with an anomalous mole-fraction behavior. The sequence determined from the reversal potential measurements may be a more accurate representation of the lobster channel because block and saturation by permeant ions should have a little effect on the reversal potential (Hille, 1992). High permeability of the lobster channel to Ca^{2+} would be novel from other Na^+-activated channels since the Na^+-sensitive cation channel from guinea pig myocytes is equally permeable to Ca^{2+} and Na^+ ($P_{Ca}/P_{Na} = 1$) (Nouailhetas et al., 1994), and Ca^{2+} does not permeate the Na^+-activated channel in crab peptidergic nerve terminals (Stuenkel et al., 1990). Although the lobster channel's relative permeability to Ca^{2+} ($P_{Ca}/P_{Na} = 39.0$), is high for this type of channel, it is still far less than that of voltage-activated L-type Ca channels ($P_{Ca}/P_{Na} \sim 1000$) (Hille, 1992). Nevertheless, it is considerably higher than the relative calcium permeability of many nonselective cation channels described so far in various tissues (*see* reviews Patridge & Swandula, 1988; Palmer, 1992, Kaupp & Altenhofen, 1992; Jonas & Burnashev, 1995). High Ca^{2+}-permeable nonselective cation channels have also been described in smooth muscle cells isolated from rat portal vein ($P_{Ca}/P_{Na} = 21$; Loirand et al., 1991) and in rat basophilic leukemia cells ($P_{Ca}/P_{Na} = 16$; Obukhov et al., 1995). Among ligand-gated channels a high Ca^{2+} permeability has been reported for N-methyl-D-aspartate (NMDA)-activated cation channels from hippocampus and spinal neurons ($P_{Ca}/P_{Na} = 10.6$; Mayer & Westbrook, 1987) and cAMP-activated nonselective cation channel from bovine ORNs ($P_{Ca}/P_{Na} = 8$; Frings et al., 1995).

The relatively high Ca^{2+}-permeability of the lobster channel may serve a specific regulatory function for the channel. We have shown previously that the activity of the lobster channel is downregulated by intracellular Ca^{2+} starting at micromolar concentrations (Zhainazarov & Ache, 1995*a*). In the absence of any downregulation, the channel presumably would be self-reinforcing, i.e., opening of the Na^+-activated channel would lead to an increase in intracellular Na^+ concentration that would lead to further rise of the channel activity. Ca^{2+} influx through the channel could provide important negative feedback to prevent the otherwise runaway self-activation of the channel by sodium.

We thank Ms. E. Wiese for help with the cell culture and Ms. L. Milstead for assistance with the figures. This work was supported by the NIDCD (DC01655).

References

Almers, W., McCleskey, E.W. 1984. Nonselective conductance in frog muscle: calcium selectivity in a single-file pore. *J. Physiol.* **353:** 585–608

Bader, C.R., Bernheim, L., Bertrand, D. 1985. Sodium-activated potassium current in cultured avian neurones. *Nature* **317:**540–542

Colquhoun, D., Hawkes, A.G. 1982. On the stochastic properties of bursts of single ion channel openings, and of clusters of bursts. *Phil. Trans. R. Soc. B.* **300:**1059

Colquhoun, D., Sakmann, B. 1981. Fluctuations in the microsecond time range of the current through single acetylcholine receptor ion channels. *Nature* **294:**464–466

Colquhoun, D., Sakmann, B. 1985. Fast events in single-channel currents activated by acetylcholine and its analogues in the frog muscle end-plate. *J. Physiol.* **369:**501–557

Colquhoun, D., Sigworth, F.J. 1995. Fitting and statistical analysis of single-channel records: *In:* Single-Channel Recording. B. Sakmann, E. Neher, editors. 2nd ed. pp. 483–587. Plenum Press, New York

Dale, N. 1993. A large, sustained Na^+- and voltage-dependent K^+ current in spinal neurons of the frog embryo. *J. Physiol.* **462:**349–372

Dyer, S.E., Fujii, J.T., Martin, A.R. 1989. A Na^+-activated K^+ current in cultured brain stem neurones from chicks. *J. Physiol.* **410:**283–296

Dryer, S.E. 1991. Na^+-activated K^+ channels and voltage-evoked ionic currents in brain stem and parasympathetic neurones from the chick. *J. Physiol.* **435:**513–532

Dryer, S.E. 1994. Na^+-activated K^+ channels: a new family of large-conductance ion channels. *Trends Neurosci.* **17:**155–160

Egan, T.M., Dagan, D., Kupper, J., Levitan, I.B. 1992*a*. Properties and run-down of sodium-activated potassium channels in rat olfactory bulb neurons. *J. Neurosci.* **12:**1964–1976

Egan, T.M., Dagan, D., Kupper, J., Levitan, I.B. 1992*b*. Na^+-activated K^+ channels are widely distributed in rat CNS and in *Xenopus* oocytes. *Brain Res.* **584:**319–321

del Castillo, J., Katz, B. 1957. Interaction at endplate receptors between different choline derivatives. *Proc. R. Soc. B. London* **146:**369–381

Fadool, D.A., Michel, W.C., Ache, B.W. 1991. Sustained primary culture of lobster (*Panulirus argus*) olfactory receptor neurons. *Tiss. Cell.* **23:**719–732

Fadool, D.A., Michel, W.C., Ache, B.W. 1993. Odor sensitivity of cultured lobster olfactory receptor neurones. *J. Exp. Biol.* **174:**215–233

Fatt, P., Ginsborg, B.L. 1958. The ionic requirements for the production of action potentials in crustacean muscle fibers. *J. Physiol.* **142:**516–543

Frings, S., Seifert, R., Godde, M., Kaupp, U.B. 1995. Profoundly different calcium permeation and blockage determine the specific function of distinct cyclic nucleotide-gated channels. *Neuron* **15:**169–179

Gorman, A.L., Thomas, M.V. 1980. Intracellular calcium accumulation during depolarization in a molluscan neurone. *J. Physiol.* **308:**259–285

Grolleau, F., Lapied, B. 1994. Transient Na^+-activated K^+ current in beating pacemaker-isolated adult insect neurosecretory cells (dum neurones). *Neurosci. Lett.* **167:**46–50.

Haimann, C., Bernheim, L., Bertrand, D., Bader, C.R. 1990. Potassium current activated by intracellular sodium in quail trigeminal ganglion neurons. *J. Gen. Physiol.* **95:**961–979

Hamill, O.P., Marty, A., Neher, E., Sakmann, B., Sigworth, F.J. 1981. Improved patch-clamp techniques for high-resolution current recording from cells and cell-free membrane patches. *Pfluegers Arch.* **391:**85–100

Harting, K. 1985. Potentiation of a transient outward current by Na^+ influx in crayfish neurones. *Pfluegers Arch.* **404:**41–44

Hatt, H., Ache, B.W. 1994. Cyclic nucleotide- and inositol phosphate-gated ion channels in lobster olfactory neurons. *Proc. Natl. Acad. Sci. USA* **91:**6264–6268

Haynes, L.W., Yau, K.W. 1990. Single-channel measurement from the cyclic GMP-activated conductance of catfish retinal cones. *J. Physiol.* **429:**451–481

Heinemann, S.H. 1995. Guide to data acquisition and analysis. *In:* Single-Channel Recording B. Sakmann, E. Neher, editors. 2nd ed. pp. 53–91. Plenum Press, New York

Hille, B. 1992. Ionic Channels of Excitable Membranes. 2nd ed. 607 pp. Sinauer Associates, Sunderland, MA

Jonas, P., Burnashev, N. 1995. Molecular mechanisms controlling calcium entry through AMPA-type glutamate receptor channels. *Neuron* **15:**987–990

Kameyama, M., Kakei, M., Sato, R., Shibasaki, T., Matsuda, H., Irisawa, H. 1984. Intracellular Na^+ activates a K^+ channel in mammalian cardiac cells. *Nature* **309:**354–356

Karpen, J.W., Zimmerman, A.L., Stryer, L., Baylor, D.A. 1988. Gating kinetics of the cyclic-GMP-activated channel of retinal rods: Flash photolysis and voltage-jump studies. *Proc. Natl. Acad. Sci. USA* **85:**1287–1291

Kaupp, U.B., Altenhofen, W. 1992. Cyclic nucleotide-gated channels of vertebrate photoreceptor cells and olfactory epithelium. *In:* Sensory Transduction. D.P. Corey, S.D. Roper, editors. pp. 133–150. The Rockefeller University Press, New York

Loirand, G., Pacaud, P., Baron, A., Mironneau, C., Mironneau, J. 1991. Large conductance calcium-activated nonselective cation channel in smooth muscle cells isolated from portal vein. *J. Physiol.* **437:**461–475

Mayer, M.L., Westbrook, G.L. 1987. Permeation and block of N-methyl-D-aspartic acid receptor channels by divalent cations in mouse cultured central neurones. *J. Physiol.* **394:**501–527

Moczydlowski, E., Latorre, R. 1983. Gating kinetics of Ca^{2+}-activated K^+ channels from rat muscle incorporated into planar lipid bilayers. *J. Gen. Physiol.* **82:**511–542

Neher, E. 1992. Correction for liquid junction potentials in patch clamp experiments. *Meths. Enzymol.* **207:**123–131

Nouailhetas, V.L.A., Aboulafia, J., Frediani-Neto, E., Ferreira, A.T., Paiva, A.C.M. 1994. A Na^+-sensitive cation channel modulated by angiotensin II in cultured intestinal myocytes. *Am J. Physiol.* **266:**C1538–C1543

Obukhov, A.G., Jones, S.V.P., Degitar, V.E., Luckhoff, A., Schultz, G., Hescheler, J. 1995. Ca^+-permeable large-conductance nonselective cation channels in rat basophilic leukemia cells. *Am. J. Physiol.* **269:**C1119–C1125

Pallotta, B.S., Magleby, K.L., Barrett, J.N. 1981. Single channel recordings of Ca^{2+}-activated K^+ currents in rat muscle cell culture. *Nature* **293:**471–474

Palmer, L.G. 1992. Epithelial Na channels: function and diversity. *Annu. Rev. Physiol.* **54:**51–66

Patridge, L.D., Swandula, D. 1988. Calcium-activated nonspecific cation channels. *Trends Neurosci.* **11:**69–72

Schoenmaker, T.J.M., Visser, G.J., Filk, G., Theuvenet, A.P.R. 1992. Chelator: an improved method for computing metal ion concentrations in physiological solutions. *Bio Techniques* **12:**994–1000

Schwindt, P.C., Spain, W.J., Crill, W.E. 1989. Long-lasting reduction of excitability by a sodium-dependent potassium current in cat neocortical neurons. *J. Neurophysiol.* **61:**233–244

Stuenkel, E.L., Ruben, P., Cooke, I.M., Lemos, J.R. 1990. Sodium-activated cation channels in peptidergic nerve terminals. *Brain Res.* **517:**35–43

Woodhull, A.M. 1973. Ionic blockage of sodium channels in nerve. *J. Gen. Physiol.* **61:**687–708

Zaykin, A., Nistri, A. 1995. A novel quabain-sensitive sodium activated cationic current of frog tectal neurones in vitro. *Soc. Neurosci. Abstr.* **21:**1818

Zhainazarov, A.B., Ache, B.W. 1995*a*. Na^+-activated nonselective cation channels in primary olfactory neurons. *J. Neurophysiol.* **73:**1774–1781

Zhainazarov, A.B., Ache, B.W. 1995*b*. Odor-induced currents in *Xenopus* olfactory receptor cells measured with perforated-patch recording. *J. Neurophysiol.* **74:**479–483

Zhainazarov, A.B., Ache, B.W. 1996. Na^+-gated cation channel from lobster olfactory receptor cells. *Chem. Senses* (*in press*)